Supplementary Information (SI) for ChemComm.
This journal is © The Royal Society of Chemistry 2026

Electronic Supplementary Information (ESI)

Defective TiO_x spontaneously triggers the hydrogenation activity of silver

Xinping Duan,*[a] Wei Zhao,[a] Zuo-Chang Chen,[a] Jianwei Zheng,[a] Haiqiang Lin,[a] Linmin Ye,[a] and Youzhu Yuan *[a]

[a] State Key Laboratory of Physical Chemistry of Solid Surfaces, National Engineering Laboratory for Green Chemical Productions of Alcohols-Ethers-Esters, and Innovation Laboratory for Sciences and Technologies of Energy Materials of Fujian Province (IKKEM), College of Chemistry and Chemical Engineering, Xiamen University, Xiamen 361005, China.

E-mail: yzyuan@xmu.edu.cn; xpduan@xmu.edu.cn

General experimental methods

Chloroauric acid ($HAuCl_4 \cdot 4H_2O$), silver nitrate ($AgNO_3$), copper nitrate ($Cu(NO_3)_2 \cdot 6H_2O$), chloroplatinic acid ($HPtCl_6 \cdot 6H_2O$), and similar reagents were of analytical grade and were obtained from the Alfa Aesar Co. (99.9% purity). The TiO_2 supports used here are anatase phase (TiO_2 (A)), P25 and rutile phase (TiO_2 (R)) respectively. TiO_2 (A) (99.8% purity) and TiO_2 (R) (99.8% purity) were purchased from Aladdin industrial corporation. P25 contains both anatase and rutile phase and was purchased from Degussa Co.

Materials and synthetic procedures.

Remarkably increasing the electrical conductivity and the density of oxygen vacancies (donor density) of TiO_2 will be engineer under reducing conditions in a reducing reagent. $NaBH_4$-treatment procotol, wherein a commonly used reducing component was selected on account of its high ability of reduction poential for transferring Ti(IV) to Ti(III), have been proposed for constructuring oxygen vacancies in metal oxides.[1, 2] The reaction mechanism is as follows:

$$NaBH_4 + 8OH^- \rightarrow NaBO_2 + 8e^- + 6H_2O \quad (1)$$

$$Ti^{4+} + e^- \rightarrow Ti^{3+} \quad (2)$$

Defective TiO_2 (anatase) was made as following processes. In detail, 1.0 g of the TiO_2 was mixed with varying contents of $NaBH_4$ to generate varied oxygen vacancies in TiO_2 under nitrogen (N_2) protection. After thoroughly grinding for 30 min, the mixtures were calcined at 350 °C for 2 h with flowing N_2 atmosphere at a heating rate of 10 °C min^{-1}. After cooling naturally to room temperature. Then the resultant solid was washed with deionized water three times to remove sodium cations, boron involved oxides and/or unreacted $NaBH_4$. The rutile TiO_2 and anatase-rutile mixed titanium oxide combined with oxygen vacancies were also made via the same methods above. The defective TiO_2 with abundant oxygen vacancies was manufactured (referred to O_v-TiO_2). [1, 2] The impurities on the TiO_2 surface were determined by elemental analysis (Inductively Coupled Plasma, ICP) and X-ray photoelectron spectroscopy (XPS). [3, 4]

Pristine and defective TiO_2 (TiO_2 and O_v-TiO_2) supported monometallic coinage metal-based catalysts with a presetting coinage metal loadings (silver, copper and gold loading of 10 wt.%, 10 wt.% and 1 wt.%, respectively) were synthesized using a conventional co-impregnation method. Specifically, taking silver-based catalyst as a instance, certain amount of $AgNO_3$ was disolved in deionized water to form a transparent solution. TiO_2 or O_v-TiO_2 solid then was introduced into the above solution. The mixture was vigorously stirred and then aged at room temperature overnight in darknees. The obtained sample was subsequently dried at 100 °C for 12 h, calcined at 350 °C for 4 h under N_2 atmosphere flow. Further, the obtained sample was divided into two parts for the undergoing catalytic assessing. It is noteworthy that the obtained Ag-O_v-TiO_2 were directly carried out on the exploration of the oxygen vacancies strightly activating silver (other coinage metals) for the selective C–O bond activation and hydrogenolysis process in dimethyl oxalate hydrogenation. On the other aspect, as a contrast, Ag-O_v-TiO_2 catalyst was further reduced in 5%H_2-95%N_2 atmosphere at 350 °C for 3 h to produce another form silver-based catalyst (donated as Ag-O_v-TiO_2). Meanwhile, pristine TiO_2 supported silver (other coinage metals, such as gold and copper) catalysts before (Ag-TiO_2) and after (Ag-TiO_2-*r*) reduction were investigated for selective C–O bond hydrogenation following the above reduction processes.

The Ag, Cu or Au loadings of the samples were determined by inductively coupled plasma optical emission spectrometer (ICP-OES) using a Thermo Elemental IRIS Intrepid II XSP. The sample was treated by aqua regia at 350 °C for 0.5 h, and the resultant solution was heated until it evaporated. The residue was diluted with 5% HCl and filtrated to a 25 mL volumetric flask before ICP-OES measurement.

Characterization methods.

The N_2 adsorption–desorption isotherms were measured at 77 K using a Micromeritics TriStar II 3020 porosimetry analyzer. The samples were degassed at 573 K for 3 h prior to measurements. The specific surface area (S_{BET}) was calculated using the Brunauer–Emmett–Teller (BET) method, in

which the isotherm data in a relative pressure (P/P_0) range of 0.05 to 0.30 were adopted. The total pore volume (V_{pore}) was derived from the absorbed N_2 volume at a relative pressure of approximately 0.99.

Powder X-ray diffraction (XRD) patterns for the catalyst samples were obtained on a PANalytical X'pert Pro diffractometer using Cu-K_α radiation (λ = 0.15418 nm) with scanning angle (2θ) ranging from 10° to 90°. The tube voltage was 40 kV, and the current was 30 mA. Each XRD pattern was identified by matching the results with reference patterns that were included in the JCPDS data base.

Transmission electron microscopy (TEM) images were obtained on a Tecnai F30 TEM operated at an acceleration voltage of 300 kV. Elemental distribution in the catalysts was determined by energy-dispersive X-ray spectroscopy (EDX) at scanning TEM (STEM) mode. The powdered catalyst was ultrasonically dispersed in ethanol at room temperature for 30 min. The as-obtained solution was then dropped into carbon-coated copper grids.

Hydrogen–temperature-programmed reduction (H_2–TPR) for the calcined catalyst samples and temperature-programmed desorption (TPD) for absorbed on the as-reduced samples were carried out on a Micromeritics Autochem II 2920 instrument connected to a Hiden Qic-20 mass spectrometer (MS). For TPR tests, 100 mg of the sample was loaded into a quartz U-tube and dried in an argon stream at 100 °C for 1 h to drive off physically adsorbed impurities. After cooling the catalysts to room temperature under an argon atmosphere, 5% H_2–95% N_2 was introduced at a rate of 50 mL min^{-1}. The temperature was then ramped linearly from the ambient temperature to 800 °C at a rate of 10 °C min^{-1}. Hydrogen consumption was simultaneously monitored using a thermal conductivity detector (TCD) and MS. For TPD tests, a beaker with 30 mL of methyl acetate and the as-reduced samples were loaded on the bottom of a glass container connected to a vacuum pump. Residual air was removed through a vacuum pump, and the as-reduced samples stayed in the methyl acetate vapor at room temperature overnight. After adsorption, the sample was loaded into a quartz U-tube, and the system was purged with high purity He for 20 min. The TPD test was conducted in flowing He (50 mL min^{-1}) with a ramping

rate of 10 °C min^{-1}. The effluent for each test was analyzed using an online mass spectrometer.

Ultraviolet–visible light (UV–vis) *diffuse reflectance spectroscopy* (DRS) of the as-reduced catalysts was collected on a UV–vis–NIR Cary 5000 scanning spectrophotometer. All catalyst precursors were freshly reduced in 5% H_2–95% N_2 atmosphere at 693 K for 3 h. The as-reduced samples were carefully protected under a nitrogen atmosphere at room temperature prior to UV–vis DRS measurements.

X-ray photoelectron spectroscopy (XPS) was performed using a JPS-9010MC photoelectron spectrometer equipped with an Al–K_α X-ray radiation source ($h\nu$ = 1486.6 eV). Prior to the measurements, each sample was pressed into a thin disk and pretreated in an atmosphere of 5%H_2–95%N_2 at 693 K for 3 h. The pretreated samples were carefully collected under nitrogen atmosphere prior to XPS measurements. The binding energy (BE) was calibrated using C 1*s* peak at 284.6 eV as reference with an uncertainty of ± 0.2 eV.

X-ray absorption fine structure (XAFS) of Ag K-edge XAFS spectra were recorded in transmission mode at room temperature, using the BL14W1 XAFS beam line at the Shanghai Synchrotron Radiation Facility. The XANES and EXAFS data reduction and analysis were performed using the Athena program that is part of the IFFEFIT software package. The filtered k^2 weighted $\chi(k)$ was Fourier-transformed into R space (k range: 2.9–14.3 $Å^{-1}$ for Ag-K EXAFS).

The Fourier-transform infrared (FT-IR) spectra of catalyst precursors and chemisorbed CO species on pre-reduced catalysts were collected on a Nicolet 6700 spectrometer at 4 cm^{-1} resolutions. In a typical procedure, 40 mg of dried catalyst was compressed into a self-supporting wafer and carefully loaded into the *in situ* cell, which was connected to a vacuum-adsorption apparatus with a residual pressure of below 10^{-4} Pa. The catalyst wafer was reduced under a flow of H_2 (50 mL min^{-1}) at 420 °C for 3 h and then evacuated for 30 min to completely remove the chemisorbed hydrogen species at the same temperature. The catalyst wafer was exposed to high-purity CO (760 Torr) for 10 min and then evacuated after cooling to 30 °C. IR spectra were collected after evacuating for 30 min and referenced to the background spectrum on

catalyst reduced at 420 prior to CO soaking under high vacuum at the same temperature.

Additionally, diffuse reflectance infrared Fourier transform spectroscopy (DRIFTS) were collected to illustrate the intrinsic interaction of C−O bound to various active sites Specifically, in situ DRIFTS spectra were recorded on Bruker Equinox 70 spectrometer equipped with MCT/A detector and operated at a resolution of 4 cm^{-1}. Before CO adsorption, the samples were pretreated with He at 120 °C for 1 h and then cooled to room temperature. The background spectrum was collected in following He and then the gas (3 vol% CO/He) was introduced into the reaction cell at a total flow rate of 33.3 mL min^{-1}. The spectra were recorded until the peak intensity was steady. The blank test was carried out following the exactly same procedure just without catalyst.

The actual contents of Ag loading were determined by X-ray fluorescence (XRF) spectroscopy. Catalyst powders were compressed into a self-supporting wafer prior to analysis, using a PANalytical AXIOS PW4400 sequential spectrophotometer with an Rh tube as radiation source. Measurements were performed with pressed pellets containing 6 wt.% wax.

Catalytic test

The catalytic performance for vapor-phase DMO hydrogenation was evaluated using a stainless steel fixed-bed tubular reactor equipped with a computer-controlled auto-sampling system [5]. Typically, 150 mg of the catalyst precursor (40-mesh to 60-mesh) was loaded into the center of the reactor, with the top side of the catalyst bed packed with quartz powder (40- to 60-mesh). Prior to catalytic performance evaluation, the catalyst was activated under a 5% H_2–95% N_2 flow at 693 K for 3 h. Then, the catalyst bed was cooled to the target reaction temperature, and pure H_2 was allowed to pass through the catalyst bed. A 10 wt.% DMO methanol solution was then pumped into the reactor using a Series III digital HPLC pump (Scientific Systems, Inc.) with a system pressure of 3.0 MPa. The outlet stream was sampled using an automatic Valco 6-port valve system and analyzed using an online gas chromatograph (Agilent 7890A) equipped with flame ionization and a KB-Wax capillary column (30 m×0.45 mm×0.85 μm) at intervals of 30 min.

The initial turnover frequency (TOF) of the reaction was measured when the DMO conversion was lower than 25%. TOF value was based on Ag or Ni dispersion obtained from XRD and TEM analyses, as well as the number of surface metal atoms according to an equation in the literature[6]. The value was calculated according to the following equation:

$$TOF = (V \times C_{DMO} \times X_{DMO})/(D \times N_M) \quad (3)$$

where V is the flow rate of the DMO methanol solution, C_{DMO} is the DMO concentration in the DMO methanol solution, X_{DMO} is the measured DMO conversion measured, D is the Ag or Ni dispersion, and N_M is the total amount of Ag or Ni. TOF indicated the moles of DMO converted per hour by each mole of the metal on the catalyst surface ($mol_{DMO}\ mol_{metal\ (surf)}^{-1}\ h^{-1}$ or simply h^{-1}).

The long-term performance of the bimetallic Ag-based catalyst was conducted under standard conditions of 3.0 MPa, 473 K, H_2/DMO = 80 (molar ratio), and 0.6 g $g_{cat}^{-1}\ h^{-1}$ weight liquid hourly space velocity (WLHSV) of DMO.

Supplemental Figures and Table

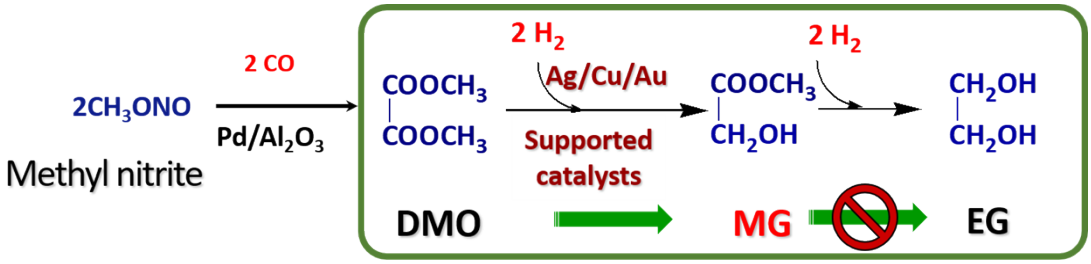

Scheme S1 Selective C–O bonds hydrogenolysis during tandem reaction over coinage metal-based catalysts.

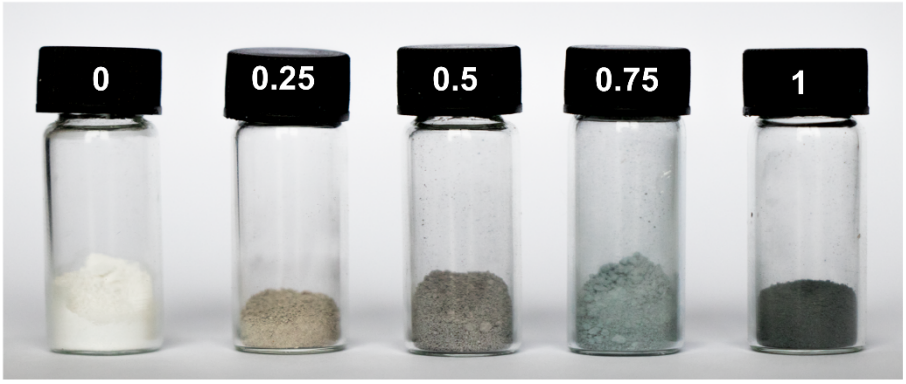

Fig. S1 Photos of TiO_2 and $NaBH_4$-treated TiO_2 nanocrystals as a function of weight ratio of $NaBH_4/TiO_2$.

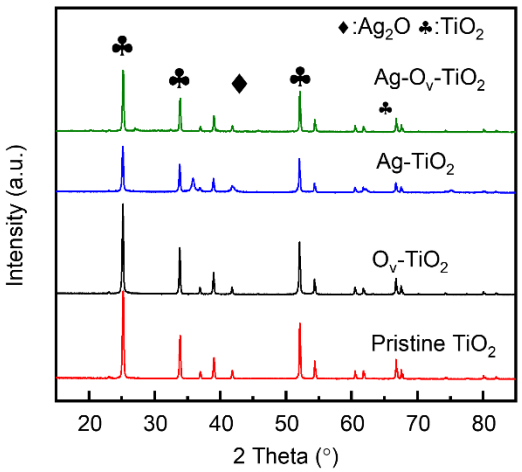

Fig. S2 XRD patterns of nanostructured anatase TiO_2 in the absence and presence of defective TiO_x overlayer, accompanied with relevant Ag-based catalysts, Ag-TiO_2 and Ag-O_v-TiO_2, respectively.

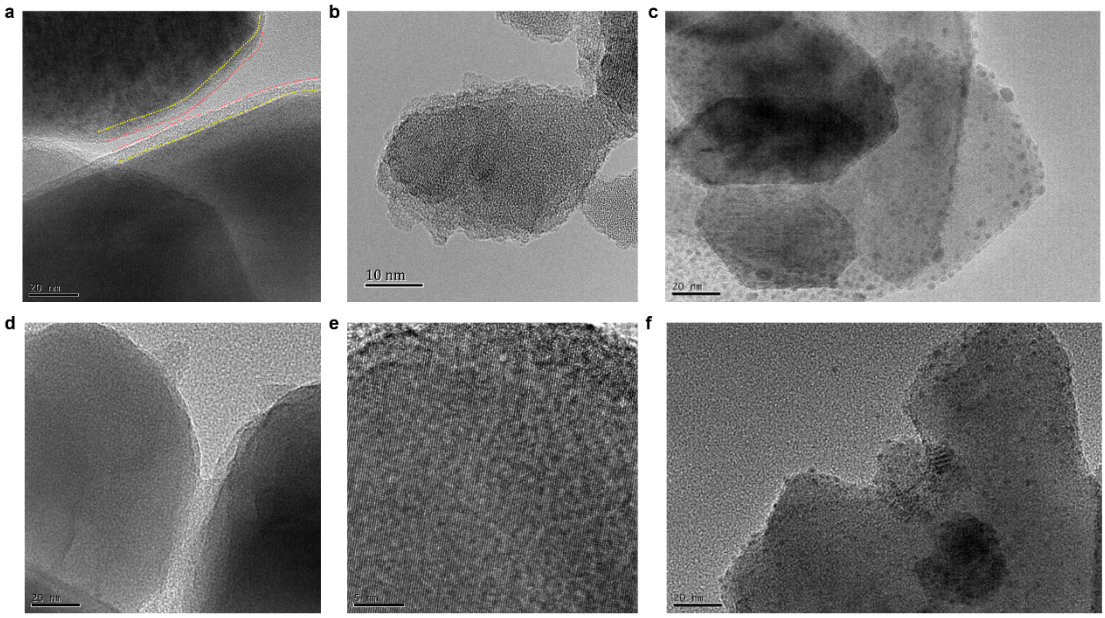

Fig. S3 HRTEM images of O_v-TiO_2 (a and b) and TiO_2 (d and e), associated with Ag-O_v-TiO_2 (c) and Ag-TiO_2 (f) catalysts.

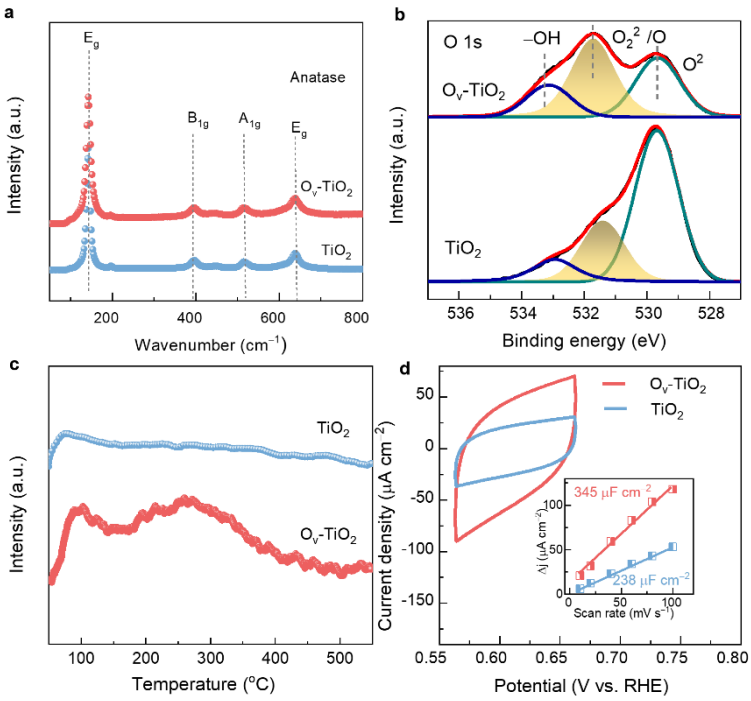

Fig. S4 Raman spectra (a), XPS spectra of identification of O 1s (b), O_2-TPD profiles (c), and CV curves of TiO_2 and O_v-TiO_2 nanocomposites (d), respectively.

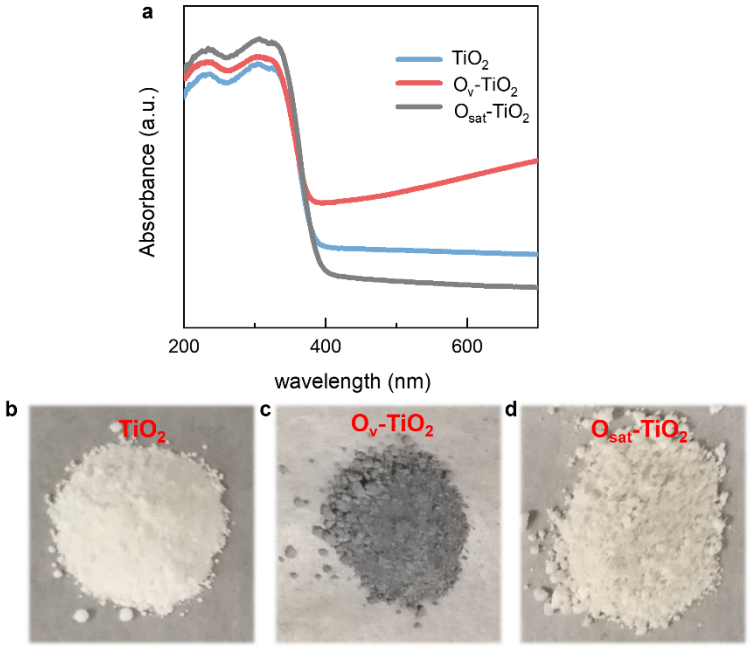

Fig. S5 UV-vis spectra (a) of TiO_2, O_v-TiO_2, and oxidized O_v-TiO_2 (O_{sat}-TiO_2) samples with corresponding photos (b-d), respectively.

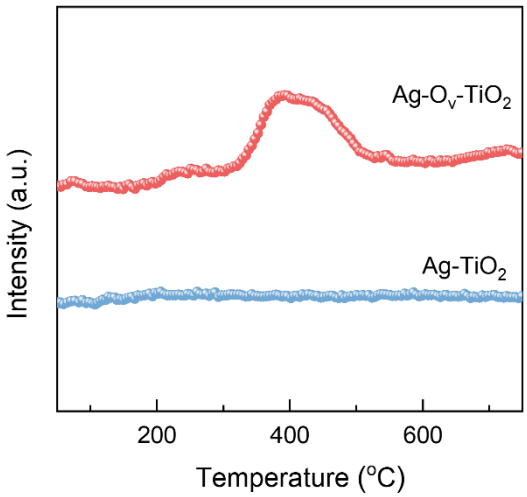

Fig. S6 CO_2-TPD profiles of Ag-TiO_2 and Ag-O_v-TiO_2 catalysts.

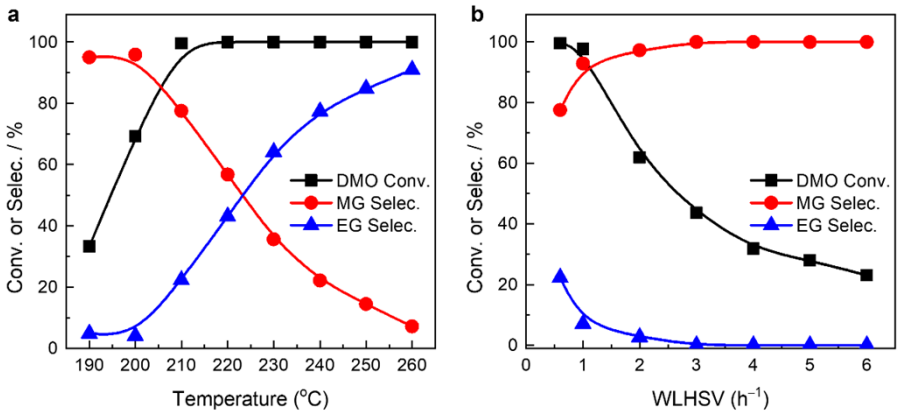

Fig. S7 Effect of reaction temperature and $WLHSV_{DMO}$ on catalytic performance with respect to Ag-O_v-TiO_2 catalyst.

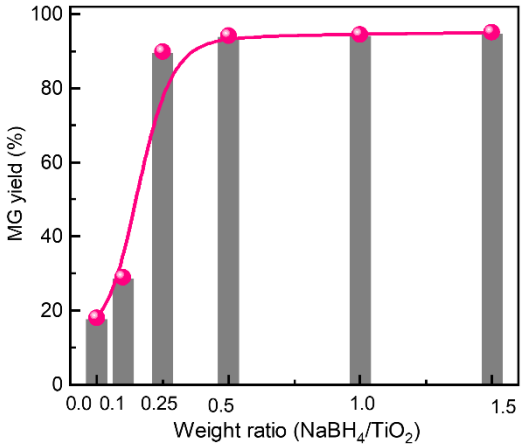

Fig. S8 MG yields of various Ag-O_v-TiO_2 catalysts obtained from distinct $NaBH_4/TiO_2$ weight ratio.

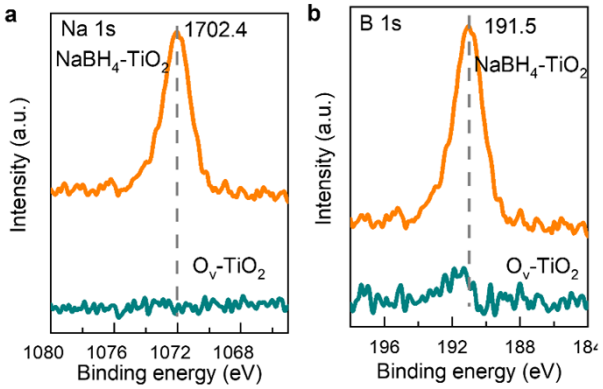

Fig. S9 XPS characteristics of B 1s (a) and Na 1s (b) illustrating the residual B and/or Na in O_v-TiO_2 nanocrystals, in comparison to the reference $NaBH_4$.

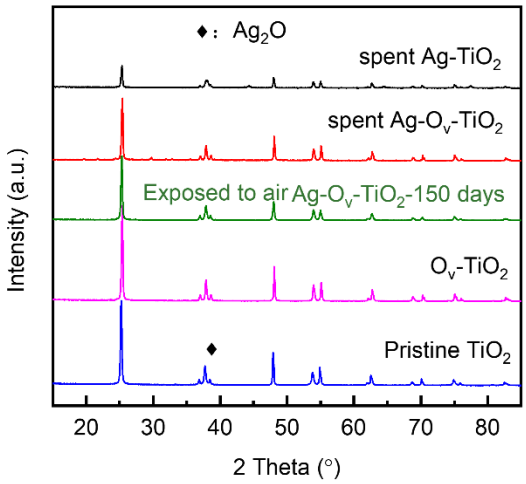

Fig. S10 XRD patterns of spent Ag-(O_v)-TiO_2 catalysts coupled with Ag-O_v-TiO_2 catalyst exposed to air for 150 days.

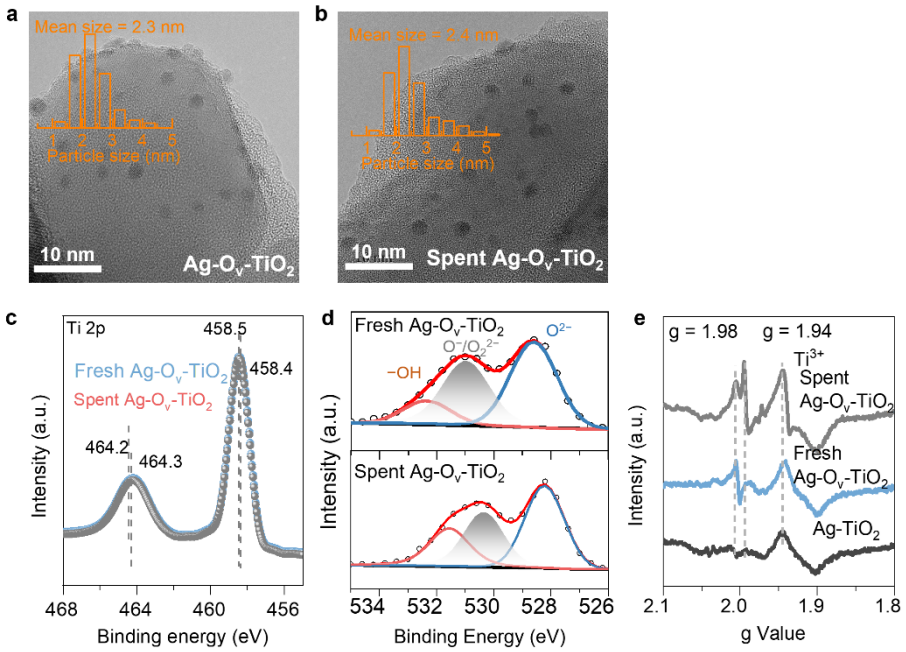

Fig. S11 HRTEM images of fresh (a) and spent (b) Ag-O_v-TiO_2 catalysts. (c) and (d) present XPS spectra of Ti 2p and deconvoluted O 1s, indicating the variation and stability of oxygen vacancies on fresh and spent Ag-O_v-TiO_2 catalysts, respectively. (e) ESR signals of fresh and spent Ag-O_v-TiO_2 catalysts.

Table S1 Structural properties of Ag-based catalysts with different TiO_2 crystalline forms.

Catalyst	BET surface area ($m^2\ g^{-1}$)	Pore volume ($cm^3\ g^{-1}$)	Pore diameter (nm)
Anatase TiO_2	48.2	0.43	26.5
O_v-TiO_2	54.6	0.46	22.8
Ag-TiO_2	36.3	0.14	16.2
Ag-O_v-TiO_2	42.7	0.21	19.8

Table S2 CO and H_2 chemisorption uptake of TiO_2- and Ag-based catalysts, determined from chemisorption.

Sample	CO uptake (μmol g_{cat}^{-1})	H_2 uptake (μmol g_{cat}^{-1})
Anatase TiO_2	0.08	0.03
O_v-TiO_2	0.7	0.6
Ag-TiO_2	3.4	0.8
Ag-O_v-TiO_2	9.8	3.6

Table S3 Curve fitting analysis results of Ag K-edge EXAFS of Ag-TiO_2 and Ag-O_v-TiO_2 and Ag foil.

Sample	Shell	N[a]	R[b] / Å	E[c]/ eV	σ^d / Å	R_f[d]
Ag foil	Ag−Ag	12	2.86	2.8	0.009	0.042
Ag-TiO_2	Ag−O	2.8±0.1	2.28	1.5	0024	0.012
	Ag−Ag	8.9±0.1	2.89	4.1	0.083	
Ag-O_v-TiO_2	Ag−O	3.6±0.1	2.26	3.6	0.081	0.006
	Ag−Ag	9.2±0.1	2.85	2.8	0.082	0.004

[a] Coordination number.

[b] Bond distance between absorber and backscatter atoms.

[c] Inner potential correction to account for the difference in the inner potentialbetween the sample and the reference compound.

[d] Debye–Waller factor.

[e] Residual factor.

Table S4. Comparison studies on catalytic performance toward DMO selective hydrogenation to MG over Ag- and Au-based catalysts

Catalyst	Tem. (°C)	H_2/DMO (mol·mol)	$WHSV_{DMO}$ ($g \cdot g_{cat}^{-1} \cdot h^{-1}$)	$Con._{DMO}$ (%)	$Sel._M$ (%)	STY_{MG} ($g_{MG} \cdot g^{-1}_{cat} \cdot h^{-1}$)	TOF (h^{-1})	Lifetime (h)	Reference
$10Ag/SiO_2$	180	150	0.5	54.4	99.8	0.21	18.3	264	[7]
Ag/MCM-41	200	100	0.2	99.8	96.2	0.15	–	–	[8]
15Ag/KCC-1	220	100	1.2	97.8	92.2	0.82	17.6	110	[9]
4.5Ag/SBA-15	235	100	0.6	99.9	95.6	0.44	19.2	–	[10]
Ag-*in*/*h*CNT	220	80	0.6	100.0	97.0	0.44	23.6	200	[11]
$15Ag/SiO_2$	220	100	0.2	100.0	92.0	0.14	12.1	120	[12]
15Ag/KCC-1	220	100	1.2	97.8	92.2	0.82	17.6	110	[9]
$Au/Fe/ZrO_2$	210	200	0.257	60.0	88.0	0.10	11.4	300	[13]
Ag/AC-N-3	220	80	0.6	99.8	95.0	0.43	–	150	[14]
10Ag/0.02Ti-KCC-1	225	100	1.0	98.0	95.0	0.73	15.7	100	[15]

Ag-B_2O_3/SiO_2	180	150	0.5	98.9	97.2	0.37	–	264	[7]
Ag/*t*-ZrO_2	205	100	1.2	60.6	97.0	0.36	21.6	100	[16]
$5Ag_1$-$Ni_{0.20}$/SBA-15	200	80	1.0	97.6	92.8	0.69	–	140	[17]
8Au-1.5Ag/SBA-15	145	100	0.6	99.5	94.2	0.43	–	200	[10]
8Au/SBA-15	235	100	0.6	65.9	99.9	0.30	–	100	[10]
0.4Ag-28CuO_x/Ni-foam	210	300	0.25	96.1	96.1	0.18	–	200	[18]
Ag-O_v-TiO_2	220	80	1.8	99.8	99.4	0.85	105.4	1000	**This work**

References

1. Q. Kang, J. Cao, Y. Zhang, L. Liu, H. Xu and J. Ye, *Journal of Materials Chemistry A*, 2013, **1**, 5766-5774.
2. Z. Xiu, Z. Xing, Z. Li, X. Wu, X. Yan, M. Hu, Y. Cao, S. Yang and W. Zhou, *Materials Research Bulletin*, 2018, **100**, 191-197.
3. J. Zhang, X. Wu, W.-C. Cheong, W. Chen, R. Lin, J. Li, L. Zheng, W. Yan, L. Gu, C. Chen, Q. Peng, D. Wang and Y. Li, *Nature Communications*, 2018, **9**, 1002.
4. G. Ou, Y. Xu, B. Wen, R. Lin, B. Ge, Y. Tang, Y. Liang, C. Yang, K. Huang, D. Zu, R. Yu, W. Chen, J. Li, H. Wu, L.-M. Liu and Y. Li, *Nature Communications*, 2018, **9**, 1302.
5. Y. Huang, H. Ariga, X. Zheng, X. Duan, S. Takakusagi, K. Asakura and Y. Yuan, *Journal of Catalysis*, 2013, **307**, 74-83.
6. J. Zhou, X. Duan, L. Ye, J. Zheng, M. M.-J. Li, S. C. E. Tsang and Y. Yuan, *Applied Catalysis a-General*, 2015, **505**, 344-353.
7. P. Schlexer, H.-Y. T. Chen and G. Pacchioni, *Catalysis Letters*, 2017, **147**, 1871-1881.
8. A. Y. Yin, C. Wen, W. L. Dai and K. N. Fan, *Applied Catalysis B-Environmental*, 2011, **108**, 90-99.
9. M. Y. Ouyang, Y. Wang, J. Zhang, Y. J. Zhao, S. P. Wang and X. B. Ma, *Rsc Advances*, 2016, **6**, 12788-12791.
10. J. W. Zheng, H. Q. Lin, Y. N. Wang, X. L. Zheng, X. P. Duan and Y. Z. Yuan, *Journal of Catalysis*, 2013, **297**, 110-118.
11. J. W. Zheng, X. P. Duan, H. Q. Lin, Z. Q. Gu, H. H. Fang, J. H. Li and Y. Z. Yuan, *Nanoscale*, 2016, **8**, 5959-5967.
12. A. Yin, X. Guo, W. Dai and K. Fan, *Chemical Communications*, 2010, **46**, 4348-4350.
13. M. Abbas, J. Zhang and J. G. Chen, *Catalysis Science & Technology*, 2020, **10**, 1125-1134.
14. R. Wang, J. Wang, H. Zi, Y. Xia, H. Wang and X. Liu, *Molecular Catalysis*, 2017, **441**, 168-178.
15. M. Y. Ouyang, J. Wang, B. Peng, Y. J. Zhao, S. P. Wang and X. B. Ma, *Applied Surface Science*, 2019, **466**, 592-600.
16. J. Zou, X. Duan, X. Liu, L. Huang, X. Liu, J. Zuo, W. Jiao, H. Lin, L. Ye and Y. Yuan, *Chemical Engineering Journal*, 2023, **454**, 140110.
17. J. F. Zhou, X. P. Duan, L. M. Ye, J. W. Zheng, M. M. J. Li, S. C. E. Tsang and Y. Z. Yuan, *Applied Catalysis a-General*, 2015, **505**, 344-353.
18. Y. F. Chen, L. P. Han, J. Zhu, P. J. Chen, S. Y. Fan, G. F. Zhao, Y. Liu and Y. Lu, *Catalysis Communications*, 2017, **96**, 58-62.